PHYSICAL REVIEW A VOLUME 50, NUMBER 6 DECEMBER 1994

Measurement of the Stark-induced amplitudes of the $6P_{1/2}\rightarrow 7P_{1/2}$ transition in atomic thallium

David DeMille, Dmitry Budker, and Eugene D. Commins
Physics Department, University of California, Berkeley, California 94720

(Received 17 May 1994)

A measurement of the Stark-induced amplitudes α and β for the $6P_{1/2}\rightarrow 7P_{1/2}$ transition in atomic thallium is reported. Absorption of cw laser light tuned to this transition at 293 nm was compared to absorption of 378-nm cw laser light tuned to the allowed $6P_{1/2}\rightarrow 7S_{1/2}$ transition. The absorption sample was an intense atomic beam in the presence of a strong electric field. The measured values are $\alpha=2.01(4)\times 10^{-5}\ \mu_B/$ (V/cm) and $\beta=1.67(4)\times 10^{-5}\mu_B/$ (V/cm), where μ_B is the Bohr magneton. These results are in agreement with semiempirical theory, but disagree with previous measurements of these amplitudes in this laboratory. A critical analysis of the previous measurement is given to explain the discrepancy. The newly measured value of β makes it necessary to reinterpret previous measurements of parity nonconservation in the $6P_{1/2}\rightarrow 7P_{1/2}$ transition. In the course of the present experiment, Stark shifts of the $6P_{1/2}\rightarrow 7P_{1/2}$ and $6P_{1/2}\rightarrow 7S_{1/2}$ transitions were also measured: $\Delta\nu(6P_{1/2}\rightarrow 7S_{1/2})=-112(6)$ kHz/(kV/cm)^2 and $\Delta\nu(6P_{1/2}\rightarrow 7P_{1/2})=-618(31)$ kHz/(kV/cm)^2. These results are also in good agrement with semiempirical theory.

PACS number(s): 32.90.+a, 32.60.+i, 32.70.Cs, 35.10.Wb

I. INTRODUCTION

The $6P_{12}\rightarrow 7P_{1/2}$ transition in Tl has been studied extensively in this laboratory because of its utility in measurements of atomic parity nonconservation. (See Fig. 1 for a diagram of the low-lying energy levels [1] of Tl.) This transition is nominally forbidden M1 with amplitude M. In the presence of an externally applied electric field $\mathbf{E}$, there are in addition Stark-induced $E1$ amplitudes α (for light polarization $\varepsilon \| \mathbf{E}$) and β (for $\varepsilon \perp \mathbf{E}$) which, for $E \gg 1$ V/cm, are much larger than M. Finally, there also exists a very small parity nonconserving $E1$ amplitude component $\mathcal{E}_P$, which arises due to the weak interaction.

Previous experiments have used interference between the dominant Stark-induced amplitudes and either $\mathcal{E}_P$ [2] or M [3] to measure the ratios $\mathcal{E}_P/\beta$, M/β, and M/α. These measurements, when initially reported, relied on theoretical determinations [4,5] of the amplitudes α and β in order to extract values for M and $\mathcal{E}_P$. Subsequently, a direct measurement of α and β was performed [6] in order to remove the contribution of the theoretical uncertainty in these quantities to the determination of $\mathcal{E}_P$ and M.

The values of α and β measured in Ref. [6] were in substantial disagreement with the calculated values. This disagreement is significant for two reasons: first, it calls into question the calculational methods used for Tl wave functions, which are also used to interpret the value of $\mathcal{E}_p$ in terms of the standard model of electroweak interactions; second, it leads to ambiguity in the extraction of $\mathcal{E}_p$ and M from experiment.

In order to resolve the existing discrepancy between theory and experiment for the Stark-induced amplitudes, α and β were remeasured using an alternative technique.

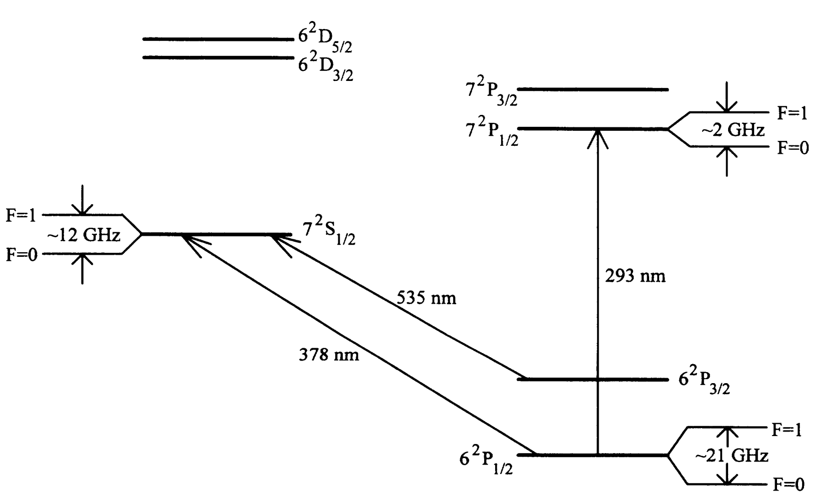

FIG. 1. Low-lying energy levels of atomic Tl (not to scale). The hyperfine splittings of ^{203}Tl and ^{205}Tl differ by only ~1%.

1050-2947/94/50(6)/4657(14)/$06.00

The absorption of cw laser light tuned to the $6P_{1/2}\rightarrow 7P_{1/2}$ transition (293 nm) was compared to the absorption of cw laser light tuned to the $6P_{1/2}\rightarrow 7S_{1/2}$ transition (378 nm), for which the A coefficient is accurately known. The absorption sample was an intense atomic beam in the presence of a large electric field. Chopping of the atomic beam and normalization of the laser powers were employed for noise and background rejection; this was critical because, even with the highest achievable beam densities and electric fields, the resonant absorption of the 293-nm light was weak ($<3\times 10^{-3}$ fractional change in light intensity). The results are in agreement with the calculated values of the Stark-induced amplitudes. This appears to indicate that the previous experimental result was subject to unconsidered systematic errors; therefore, a critical analysis of the previous measurement [6] will be given.

In the course of the work on the Stark-induced amplitudes, Stark shifts in the $6P_{1/2}\rightarrow 7P_{1/2}$ and $6P_{1/2}\rightarrow 7S_{1/2}$ transitions were measured. These measurements provide additional checks of calculations involving Tl wave functions.

A. Stark-induced amplitudes and energy shifts

In the one-electron central field (OECF) approximation, the presence of an external electric field $\mathbf{E}$ induces an $E1$ transition amplitude between the states $6P_{1/2}$ and $7P_{1/2}$ which takes the form

$$\mathcal{E}_{\text{Stark}}=e^2\left\{\sum_{m\neq 7P_{1/2}}\frac{\langle 7P_{1/2}|\mathbf{E}\cdot\mathbf{r}|m\rangle\langle m|\boldsymbol{\varepsilon}\cdot\mathbf{r}|6P_{1/2}\rangle}{E_{7P_{1/2}}-E_m}+\sum_{m\neq 6P_{1/2}}\frac{\langle 6P_{1/2}|\mathbf{E}\cdot\mathbf{r}|m\rangle\langle m|\boldsymbol{\varepsilon}\cdot\mathbf{r}|7P_{1/2}\rangle}{E_{6P_{1/2}}-E_m}\right\}, \tag{1}$$

where $\boldsymbol{\varepsilon}$ is the polarization of the light field. There are two independent Stark-induced amplitudes $\alpha|\mathbf{E}|$ and $\beta|\mathbf{E}|$ corresponding to $\boldsymbol{\varepsilon}\|\mathbf{E}$ and $\boldsymbol{\varepsilon}\perp\mathbf{E}$, respectively. In the OECF approximation, evaluation of the angular factors in the sums yields

$$\begin{aligned}\alpha=&\tfrac{1}{9}e^2\sum_{nS_{1/2}}R_{7P,nS}R_{6P,nS}\left[\frac{1}{E_{7P_{1/2}}-E_{nS_{1/2}}}+\frac{1}{E_{6P_{1/2}}-E_{nS_{1/2}}}\right]\\&+\tfrac{2}{9}e^2\sum_{nD_{3/2}}R_{7P,nD}R_{6P,nD}\left[\frac{1}{E_{7P_{1/2}}-E_{nD_{3/2}}}+\frac{1}{E_{6P_{1/2}}-E_{nD_{3/2}}}\right]\end{aligned} \tag{2}$$

and

$$\begin{aligned}\beta=&\tfrac{1}{9}e^2\sum_{nS_{1/2}}R_{7P,nS}R_{6P,nS}\left[-\frac{1}{E_{7P_{1/2}}-E_{nS_{1/2}}}+\frac{1}{E_{6P_{1/2}}-E_{nS_{1/2}}}\right]\\&+\tfrac{1}{9}e^2\sum_{nD_{3/2}}R_{7P,nD}R_{6P,nD}\left[\frac{1}{E_{7P_{1/2}}-E_{nD_{3/2}}}-\frac{1}{E_{6P_{1/2}}-E_{nD_{3/2}}}\right],\end{aligned} \tag{3}$$

where $R_{6P,nS}=\langle 6P_{1/2}|r|nS_{1/2}\rangle$, etc. are radial integrals. These amplitudes were calculated in Ref. [4] using a Green's-function technique, which effectively includes the sum over all discrete, continuum, and autoionizing states. The results of this calculation were

$$\begin{aligned}\alpha&=2.05(30)\times 10^{-5}\mu_B/(\text{V/cm})\,,\\ \beta&=1.64(25)\times 10^{-5}\mu_B/(\text{V/cm})\,.\end{aligned} \tag{4}$$

The applied electric field also induces second-order energy shifts which, in the OECF approximation, can be written as

$$\Delta E_{nP_{1/2}}=e^2|\mathbf{E}|^2\left\{\frac{1}{9}\sum_{mS_{1/2}}\frac{|\langle mS_{1/2}|r|nP_{1/2}\rangle|^2}{E_{nP_{1/2}}-E_{mS_{1/2}}}+\frac{2}{9}\sum_{mD_{3/2}}\frac{|\langle mD_{3/2}|r|nP_{1/2}\rangle|^2}{E_{nP_{1/2}}-E_{mD_{3/2}}}\right\}, \tag{5}$$

$$\Delta E_{nS_{1/2}}=e^2|\mathbf{E}|^2\left\{\frac{1}{9}\sum_{mP_{1/2}}\frac{|\langle mP_{1/2}|r|nS_{1/2}\rangle|^2}{E_{nS_{1/2}}-E_{mP_{1/2}}}+\frac{2}{9}\sum_{mP_{3/2}}\frac{|\langle mP_{3/2}|r|nS_{1/2}\rangle|^2}{E_{nS_{1/2}}-E_{mP_{3/2}}}\right\}. \tag{6}$$

The Stark shift of the ground state ($6P_{1/2}$) has been previously calculated using semiempirical wave functions and including contributions from core-excited autoionizing states [7]

$$\Delta E_{6P_{1/2}}=-12(2)\ \text{kHz/(kV/cm)}^2\,. \tag{7}$$

To the best of our knowledge, no calculations of Stark shifts of excited states of Tl have appeared in the literature. Using the calculated values of the radial matrix elements $\langle r\rangle$ for low-lying states which are tabulated in Ref. [4] and also the experimentally determined energies (from Ref. [1]), the sums of Eqs. (5) and (6) can be numerically approximated. These calculations yield [8]

$$\Delta E_{7P_{1/2}} = -624(130)\ \text{kHz}/(\text{kV}/\text{cm})^2 , \tag{8}$$

$$\Delta E_{7S_{1/2}} = -116(30)\ \text{kHz}/(\text{kV}/\text{cm})^2 . \tag{9}$$

The uncertainties quoted here are dominated by the uncertainties in the values of the radial matrix elements from Ref. [4] (10%), but also include the uncertainties arising from the omission of highly excited states (including core-excited states) in the sums of Eqs. (5) and (6).

B. Determination of Stark amplitudes from the relative absorption measurement

The near-resonant absorption of light by a sample of atoms can be written in the general form

$$\frac{I_{\text{transmitted}}}{I_{\text{incident}}} = e^{-\mu(\nu-\nu_0)} , \tag{10}$$

where the frequency-dependent absorption factor $\mu(\nu-\nu_0)$ can be expressed in the form (see, e.g., Ref. [9])

$$\mu(\nu-\nu_0) = \kappa \nu_{if} g(\nu-\nu_0) \int n(x)dx . \tag{11}$$

Here ν_{if} is the frequency of the transition from initial state i to final state f; $g(\nu-\nu_0)$ is the line-shape function, normalized to unit area; $n(x)$ is the (position-dependent) density of atoms in the sample; and κ, referred to as the line strength, is given by

$$\kappa \equiv (2\pi)^2 \alpha_{\text{FS}} \sum_{g_i, g_f} |\langle f, g_f | \boldsymbol{\varepsilon}\cdot\mathbf{r} | i, g_i \rangle|^2 F(g_i) , \tag{12}$$

where α_{FS} is the fine-structure constant, g_i (g_f) is a label which enumerates the degenerate sublevels of level i (f), and $F(g_i)$ is fraction of the total population in sublevel g_i.

For the determination of the Stark-induced amplitudes, the advantage of a relative absorption measurement between the Stark-induced transition and a reference transition is that the column density $\int n(x)dx$ need not be determined since it cancels in the ratio of absorptions (μ'/μ). Note, however, that the function $g(\nu-\nu_0)$ is not the same for two different transitions; in particular, the peak values of the line-shape functions for the two transitions are different. This means that in order to extract the desired ratio of transition matrix elements from a relative absorption measurement, it is necessary to know not only the ratio of peak absorptions, but also the ratio of the peak values of the line-shape functions. This point will be returned to below and in Sec. III B.

The line strength for the reference transition $6P_{1/2}\rightarrow 7S_{1/2}$ can be cast conveniently in terms of the A coefficient for this transition. This is done by using the easily derived relation (see, e.g., Ref. [4])

$$A(7S_{1/2}\rightarrow 6P_{1/2}) = \frac{4}{9}(2\pi)^3 \frac{\alpha_{\text{FS}}\nu^3_{7S_{1/2}\rightarrow 6P_{1/2}}}{c^2} \langle r_{7S_{1/2},6P_{1/2}} \rangle^2 . \tag{13}$$

The A coefficient for the transition $7S_{1/2}\rightarrow 6P_{1/2}$ in Tl (378 nm) is known from the total A coefficient for the $7S_{1/2}$ state [10] and the branching ratio [11] of $7S_{1/2}\rightarrow 6P_{1/2}$:

$$A(7S_{1/2}\rightarrow 6P_{1/2}) = 6.13(16)\times 10^7\ \text{s}^{-1} . \tag{14}$$

Taking into account the hyperfine structure of each level (both ^{205}Tl and ^{203}Tl have nuclear spin $I=\frac{1}{2}$) and evaluating the angular factors in the expression for the line strengths κ [Eq. (12)], one finds

$$\begin{aligned}\kappa(6P_{1/2}, F=1\rightarrow 7S_{1/2}, F'=0) &= (2\pi)^2\alpha_{\text{FS}} \frac{\langle r_{6P_{1/2},7S_{1/2}}\rangle^2}{9} \times \frac{1}{4} \\ &= \frac{c^2}{32\pi\nu^3_{6P_{1/2}\rightarrow 7S_{1/2}}} A(7S_{1/2}\rightarrow 6P_{1/2}) ,\end{aligned} \tag{15}$$

where the factor of $\frac{1}{4}$ accounts for the thermal distribution of the population among the hyperfine sublevels of the $6P_{1/2}$ level. Similarly, the line strengths for the Stark-induced transition (293 nm) can be evaluated, yielding

$$\begin{aligned}\kappa(6P_{1/2}, F=1\rightarrow 7P_{1/2}, F'=1; \boldsymbol{\varepsilon}\|\mathbf{E}) &= \frac{3}{4}\frac{(2\pi)^3}{hc}\alpha^2 E^2 , \\ \kappa(6P_{1/2}, F=1\rightarrow 7P_{1/2}, F'=1; \boldsymbol{\varepsilon}\perp\mathbf{E}) &= \frac{1}{2}\frac{(2\pi)^3}{hc}\beta^2 E^2 .\end{aligned} \tag{16}$$

Using Eqs. (11), (15), and (16), the desired quantities α^2 and β^2 can be written in a form which depends only on quantities which are either previously known or measured in this experiment, i.e., the applied electric field, the ratio of peak absorptions, the ratio of the peak values of the line-shape functions, the transition wavelengths, and the A coefficient of the $7S_{1/2}\rightarrow 6P_{1/2}$ transition. For example,

$$\begin{aligned}\alpha^2 = \frac{1}{E^2} & \frac{\mu_{293}|_{\text{peak}}(F=1\rightarrow F'=1; \boldsymbol{\varepsilon}\|\mathbf{E})}{\mu_{378}|_{\text{peak}}(F=1\rightarrow F'=0)} \frac{293}{378} \frac{g_{378}|_{\text{peak}}}{g_{293}|_{\text{peak}}} \\ & \times \frac{h}{192\pi^4} \lambda^3_{6P_{1/2}\rightarrow 7S_{1/2}} A(7S_{1/2}\rightarrow 6P_{1/2}) .\end{aligned} \tag{17}$$

This is the expression used to determine the Stark-induced amplitude α from the ratio of peak absorptions.

II. APPARATUS

The Stark-induced transition is, for achievable laboratory electric fields, much weaker than the $6P_{1/2}\rightarrow 7S_{1/2}$ transition. Assuming that the ratio of peak values of the line-shape functions is of order unity (as is the ratio of transition frequencies), Eq. (11) shows that the ratio of peak absorption coefficients is given approximately by the ratio of line strengths. Using the expressions of Eqs. (15) and (16) for the line strengths, as well as Eq. (14) for the $7S_{1/2}\rightarrow 6P_{1/2}$ A coefficient and Eq. (4) for the theoretical value of α, the ratio of the 293-nm absorption coefficient to the 378-nm absorption coefficient can be estimated. This ratio is found to be only $\sim 3\times 10^{-4}$ for $E=100$ kV/cm. Thus, in order to produce the largest

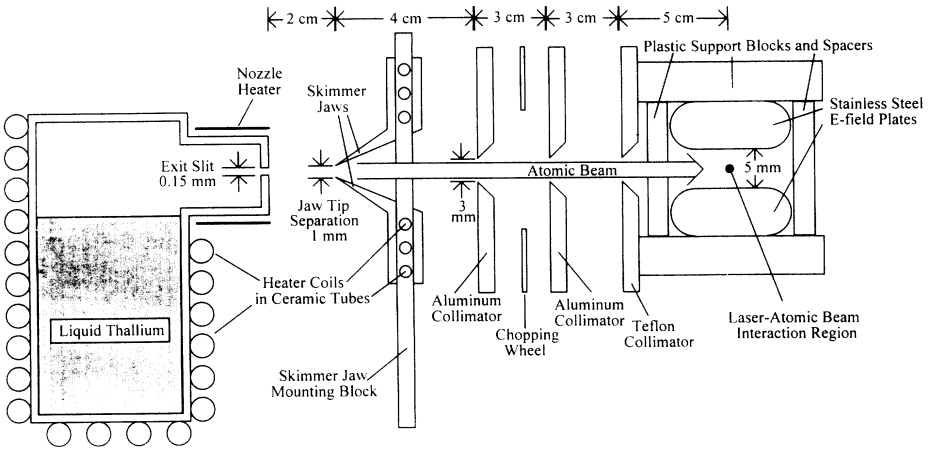

FIG. 2. Schematic depiction of the atomic beam oven, collimators, and interaction region. All distances shown are approximate.

possible absorption coefficient on the weak Stark-induced transition, it was attempted to maximize both the column density of the atomic beam and the ability to sustain a large electric field in the presence of the dense beam. The following sections will describe in detail the relevant features of the atomic-beam apparatus (shown in Fig. 2) and the high-voltage electric-field system used to achieve this goal. In addition, the optical setup (shown in Fig. 3) and data collection and processing used for the absorption measurements will be described.

A. Atomic beam

The oven used to produce the atomic beam was constructed from tantalum sheet, fit together in the shape of a rectangular box with a volume of ~ 500 cm^3. The box was sealed by arc welding in an argon atmosphere. The oven body was resistively heated with heaters constructed from coiled tantalum wire held in ceramic tubes and was surrounded with three layers of shielding to reduce radiative heat loss. The use of high-purity alumina ceramic was found to be essential to avoid a chemical reaction

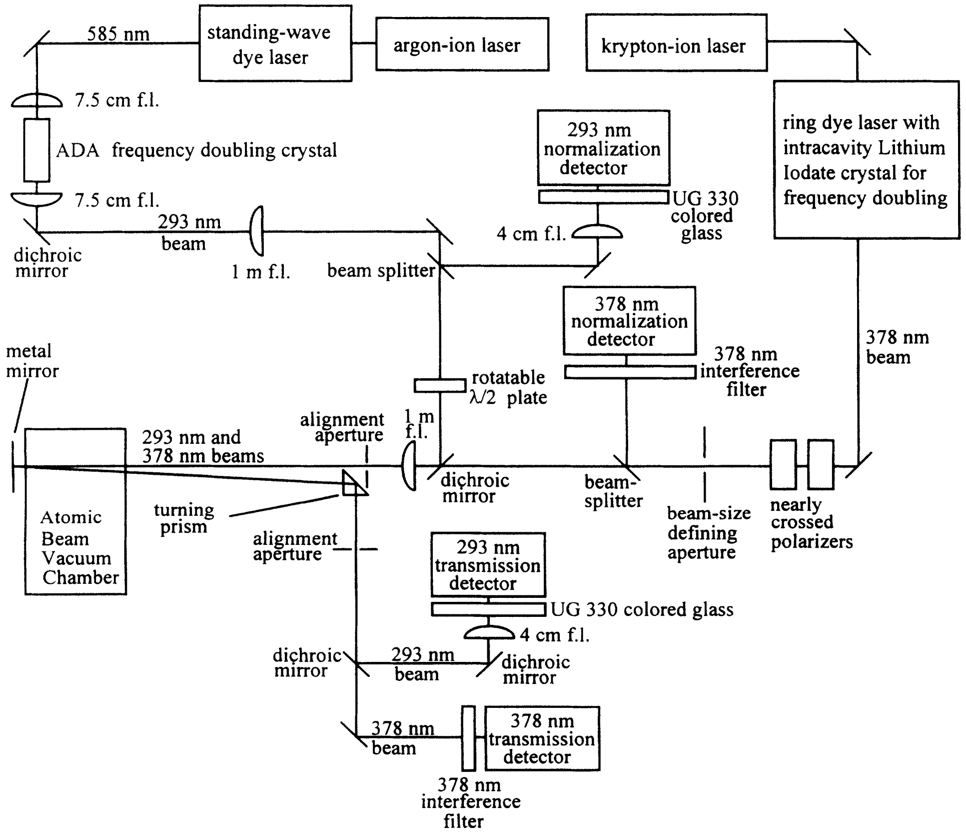

FIG. 3. Lasers and optics used for the relative absorption measurement.

which destroyed the heaters at their points of contact with the insulators.

The oven exit orifice was a slit 0.6 mm deep, 0.15 mm high ×13 mm long. The slit was cut into the end of a sealed tube which extended from the oven body. This allowed the slit to be heated separately from the body to ensure that it was not the coldest part of the oven and did not clog due to thallium condensation; it was typically maintained at least 75° C hotter than the body. The slit tube heater was constructed from a single piece of molybdenum foil wrapped around a high-purity alumina tube. The entire tube assembly was covered with four layers of tantalum foil for radiative heat shielding. The sheet heater design was chosen to minimize the voltage on the heater at a given power so as to avoid the possibility of discharge in the dense thallium vapor just outside the exit slit.

The oven body was typically maintained at $\sim 1100\,^{\circ}\mathrm{C}$, corresponding to a Tl vapor pressure of ~ 50 Torr. At this pressure, the beam was beyond the effusive regime and well into the continuum-flow regime of operation. Under these conditions, the material output of the oven was ~ 20 g/h.

Collimation of the atomic beam was necessary to avoid thallium deposition on the electric-field plates in the laser–atomic-beam interaction region (see below). However, the large material output of the oven described here could quickly clog a collimating slit on which the thallium could condense and solidify. Because of this, a provision was made to heat the initial collimator (skimmer) and also to have the dimensions of the holes of the following (cold) collimators substantially larger than that of the first.

Generally, it is known that the use of a noncondensing collimator to avoid clogging limits the useful flux from a continuum-flow beam source [12]. This is believed to be due to collisions between beam atoms and atoms backscattered from the collimator. In the present work, the collimator was maintained at a temperature somewhat above the thallium melting temperature (300 °C), where the thallium vapor pressure is low ($< 10^{-6}$ Torr). In this regime, it was found that a considerable fraction of the beam flux condensed on the collimator, which reduced backscattering; at the same time, the liquid condensed thallium could drain away from the collimating slit without permanently clogging it.

In the particular geometric arrangement of our beam and collimator, it was found that the first collimator remained above the thallium melting temperature with no power directly applied to the collimator; the absorbed radiative power from the oven was sufficient. The actual ambient temperature of the skimmer under running conditions was not measured because thermocouple leads became immediately fouled with thallium condensation. In this skimmer temperature regime, it was also observed that the absorption signal was subject to intermittent rapid jumps of up to 10% every few tens of seconds; this was likely due to passage of liquid thallium droplets into or out of the skimmer slit. In the comparison between absorption on the two transitions, however, these variations were canceled; thus no effort was made to remedy this situation.

The first collimator was constructed from two separate knife-edged stainless-steel jaws with surfaces at a small angle to the beam direction (see Fig. 2). This "skimmer"-type jaw configuration was an attempt to minimize specular-reflection backscattering. Because of the rectangular beam geometry, "skimming" collimation (i.e., with a collimating surface which is knife edged and at near-grazing angles to the beam) was possible only in the short (vertical) dimension; the only collimation provided in the long (horizontal) direction was from the flat surfaces of the mounting block, which left a horizontal opening of 25 mm. The jaws themselves were 20 mm long in the horizontal dimension; the tip separation was 1 mm. Each jaw was hung from ceramic tubes mounted in holes in a stainless-steel block. The mounting block was surrounded by a sheet of stainless-steel foil to collect the thallium emitted from the oven at large angles as well as that scattered from the skimmer. The foil was shaped in such a way as to funnel liquid thallium into a collector cup placed under the skimmer. (The solidified thallium from the cup was periodically melted into the oven for reuse).

Following the skimmer, three additional collimators (3 mm high, 30 mm wide; 2 aluminum, 1 Teflon) were installed in the beam path before the electric-field plates. These collimators prevented any direct geometrical path from the open aperture of the skimmer to any part of the plates. The collimators had flat front surfaces, but were machined with knife-edged holes in an attempt to limit scattering. In addition, the ambient temperature of these collimators was sufficiently low that thallium could both condense and solidify on them. Nevertheless, the traces of thallium deposition indicated that some thallium was scattered at angles of up to $\sim 10^{\circ}$ after each collimator surface. This meant that there was still substantial deposition of thallium on the electric-field plates in the interaction region. While this deposition was not sufficient to noticeably change the spacing between the electric-field plates, it did eventually lead to high-voltage discharges between the plates. (These discharges took the form of a low-current quasi-dc component plus occasional high-current bursts.) In addition, the first collimator after the skimmer eventually showed substantial clogging in the vertical (narrow) dimension. For these reasons, the time of each run was limited to $\lesssim 8$ h. Following each run, the vacuum system was opened and thallium was cleaned off the collimators and electric-field plates.

An atomic-beam chopper was a crucial element of the absorption measurements. The ability to compare signal with the atomic beam open to that with it closed has a number of advantages over a system where the optical thickness of the absorbing sample cannot be modulated. Most importantly, nearly all absorption effects unrelated to the atoms under study are canceled in the ratio of beam-open to beam-closed signal.

The beam chopper was located between the first two cold collimators. It was driven via a ferrofluidic rotary vacuum feedthrough by a stepping motor at 13.5 rps. The chopper had five vanes.

The entire beam apparatus was inside a vacuum chamber pumped by a diffusion pump and a liquid-nitrogen cold trap. The residual pressure with the oven at operating temperature was typically $\sim 10^{-5}$ Torr; noticeable attenuation of the beam occurred if the chamber pressure rose above $\sim 3\times10^{-5}$ Torr.

B. Lasers and optics

Two lasers were used in the absorption measurements. The 378-nm light used to measure absorption on the $6P_{1/2}\rightarrow7S_{1/2}$ transition was produced by intracavity doubling with a $LiIO_3$ crystal of the fundamental beam of a ring dye laser (Coherent CR699-21). The dye laser operated with LD700 dye and was pumped by ~ 6 W from the red lines of a Kr^+ laser (Coherent Innova 100-K3). The dye laser operates in a single mode and has active frequency stabilization. This provides a nominal linewidth of 1 MHz in the uv output. Typically, 3–5 mW of 378-nm light were produced. The beam was linearly polarized.

In order to perform the relative absorption measurements, it was important that the 378-nm beam have very small power to avoid optical pumping effects and also that it have a shape and size which approximated that of the 293-nm beam. In order to accomplish this, the 378-nm beam was passed through an iris diaphragm to match its size to that of the 293-nm beam. After the aperture, the beam passed through two nearly crossed polarizers which attenuated the power to $\lesssim 5$ nW. After the polarizers, the beam passed through a 50-50 beam splitter. The transmitted beam traveled directly into a photomultiplier tube used for normalization of the laser power, while the reflected beam traveled on to the interaction region with the atomic beam.

The 293-nm light used to measured absorption on the Stark-induced $6P_{1/2}\rightarrow7P_{1/2}$ transition was also produced by frequency doubling. The fundamental beam at 585 nm was produced by a single-mode, actively stabilized standing-wave dye laser (Coherent CR599-21) using Rhodamine 6G pumped by ~ 4.5 W (all lines) from an Ar^+ laser (Coherent Innova 70). The 585-nm output beam, with a typical power of ~ 100 mW and a nominal linewidth of 1 MHz, was focused with a 7.5-cm focal length lens into a 5-cm-long temperature-tuned ammonium dihydrogen arsenate (ADA) crystal. The 293-nm beam had typical power ~ 500 nW and a roughly TEM_{00} transverse mode structure. The beam was linearly polarized.

The diverging 293-nm beam emerging from the crystal was recollimated and sized with two lenses. After reflections by a series of mirrors, the beam passed through a 50-50 beam splitter. One of the resulting two beams was incident on a photodiode used for normalization of the laser power. The other beam, which was used to measure absorption, passed through a $\lambda/2$ plate which could be adjusted to rotate the linear polarization of the light. The quality of the linear polarization was checked several times throughout the lifetime of the apparatus by noting the ratio of maximum to minimum transmission through a polarizer placed after the $\lambda/2$ plate; this ratio was $<7\times10^{-3}$.

After the $\lambda/2$ plate, the 293-nm beam was reflected from a dichroic mirror which was used to spatially combine it with the 378-nm beam. The positions, angles, and sizes of the two beams were matched at this mirror visually (using a fluorescent card); the beams were roughly circular in cross section with 2 mm diameter. The overlapped beams then passed through a 1-m focal length fused silica lens. The region of overlap with the atomic beam was ~ 75 cm from the lens. On the other side of the vacuum chamber, near the focal point of the lens, a mirror reflected both beams back through the vacuum chamber at a small angle to the incident direction. After the passage of the two beams through the vacuum chamber, a dichroic mirror separated the two wavelengths; the 293-nm beam was reflected into a photodiode, while the transmitted 378-nm beam passed into a photomultiplier tube.

The beams were focused in the interaction region because of the danger of systematic effects in the relative absorption measurement due to inhomogeneity in the atomic beam. The small laser beam sizes help to mitigate these effects. Because of diffraction, the waist size of the beams in the interaction region was $\gtrsim 0.1$ mm (the actual sizes were not determined). Assuming that the beam waist was given by the diffraction-limited minimum, it was necessary to limit the 378-nm power to $P_{378} < 5$ nW in order to ensure that less than 1% of the atomic beam could be optically pumped to nonabsorbing states. In addition to maintaining this limit during all data taking, it was also confirmed that the 378-nm absorption did not change noticeably when the 378-nm power was increased by a factor of 10 over the usual level. (Because the line strength of the 293-nm transition is, for the maximum available electric field of 100 kV/cm, $<3\times10^{-4}$ of the line strength of the 378-nm transition, the corresponding limit for the 293-nm power was $P_{293} < 15\mu$W; the available power was less than this limit.)

To block out stray light, the input windows of the 378-nm detecting photomultiplier tubes (PMTs) were covered with 378-nm interference filters, while the input windows of the 293-nm-detecting photodiodes were covered with uv transmitting, visible absorbing colored glass (Hoya U330). The alignment of the beams relative to the electric field was set with a series of fixed apertures to within 2°. The alignment of the 293-nm polarization relative to the electric field was checked via the angular dependence of the Stark-induced signal (see Sec. III D).

C. Detection electronics and data collection

The 378-nm light beams were detected by PMTs, while the 293-nm light beams were detected by photodiodes. The use of different detectors was due to the different power levels used at the two wavelengths.

The PMTs (EMI 9750QB) used for 378-nm detection were adjusted to give a gain of $\sim 4\times10^4$. The outputs of the PMTs were sent to preamplifiers and then to adjustable gain dc amplifiers to ensure that the full dynamic range of the electronics system could be used, thus allowing accurate measurement of large absorptions. The 378-nm transmission and normalization signals will be referred to as S_{t378} and S_{n378}, respectively.

The 293-nm light beams were detected by uv-sensitive photodiodes with built-in preamplifiers (UDT 455UV). The outputs of the preamplifiers were each sent to adjustable gain dc amplifiers; the outputs of the amplifiers (S_{t293} and S_{n293}, defined as for the 378-nm beams) were sent to averaging and differencing circuits which produced the output signals

$$\begin{aligned} S_{a293} &= [S_{t293}+S_{n293}]/2 \ , \\ S_{d293} &= 100[S_{t293}-S_{n293}] \ . \end{aligned} \tag{18}$$

The gain of each channel in the averaging circuit was determined by feedback resistors to within 0.5%; the gain of the differencing circuit was determined to 0.1% by the use of a precision instrumentation amplifier (Analog Devices AD624C). During data taking, the difference signal tended to drift slowly away from zero; this was believed to be due primarily to thallium deposition on the vacuum windows which gave rise to gradually increasing absorption of the transmitted beam. The gains of each channel were adjusted every few minutes to rezero the output (see below). The four signals S_{t378}, S_{n378}, S_{a293}, and S_{d293} were all sent to gated integrators, with gates synchronized to the atomic-beam chopping wheel (see below). The outputs of the gated integrators were digitized by 12-bit analog-to-digital converters (ADCs) (IBM Data Acquisition and Control Board). For all channels, the ADC zero level due to small dc offsets in the electronics chain was determined by measurements with laser light blocked; this zero level was subtracted from each of the four digitized signals before storage in the computer.

The data taking was synchronized to the position of the chopper by using the signals from a digital encoder attached to the chopper drive shaft. The half-cycle time of the beam chop was 7.5 ms. A delay of ~2.5 ms between the opening of the beam and the beginning of the gate pulse to the gated integrator was included to allow the photodetector preamplifiers (with RC time 500 μs) to settle to a value within 1% of their dc level. The gate was then opened for ~3 ms. This left ~2 ms for the computer to digitize and store the signals.

The density of the atomic beam was sufficient to produce several absorption lengths on the 378-nm transition. Therefore, the absorption coefficient of 378-nm light due to the $6P_{1/2}\rightarrow 7S_{1/2}$ transition was determined from the relation

$$\mu_{378} = -\ln \left[\frac{\left. \left[\dfrac{S_{t378}}{S_{n378}} \right] \right|_{\text{beam open}}}{\left. \left[\dfrac{S_{t378}}{S_{n378}} \right] \right|_{\text{beam closed}}} \right] \ . \tag{19}$$

The absorption of 293-nm light due to the Stark-induced $6P_{1/2}\rightarrow 7P_{1/2}$ transition was determined from the relation

$$\mu_{293} = -\frac{1}{100} \left[\left. \left[\frac{S_{d293}}{S_{a293}} \right] \right|_{\text{beam open}} - \left. \left[\frac{S_{d293}}{S_{a293}} \right] \right|_{\text{beam closed}} \right] \ , \tag{20}$$

where the factor of 100 accounts for the gain in the differencing circuit. The use of this relation requires both that the beam-dependent 293-nm absorption coefficient be $\ll 1$ and that the signal sizes in the transmission and normalization channels be matched. Defining the quantities μ_{Tl} (the atomic beam-dependent absorption coefficient for 293-nm light) and ε (the signal size mismatch) such that

$$\mu_{\text{Tl}} \equiv -\ln \left[\frac{S_{t293}|_{\text{beam open}}}{S_{n293}|_{\text{beam open}}} \right] \tag{21}$$

and

$$\varepsilon \equiv \left[\frac{S_{t293}|_{\text{beam closed}}}{S_{n293}|_{\text{beam closed}}} \right] - 1 \ , \tag{22}$$

it can be shown that the relations of Eqs. (20) and (18) yield, as desired,

$$\mu_{293} = \mu_{\text{Tl}}[1+O(\varepsilon^2, \varepsilon\mu_{\text{Tl}}, \mu_{\text{Tl}}^2)] \ . \tag{23}$$

During data taking, ε was maintained to be $<5\times 10^{-3}$ by occasional adjustment of the gains of each channel. In addition, the atomic-beam-dependent absorption μ_{Tl} was $<3\times 10^{-3}$. Thus Eq. (20) determines μ_{293} with negligible corrections. In addition, the relation of Eq. (20) removes spurious absorption backgrounds which do not depend on the presence of the atomic beam, as well as noise due to fluctuations in laser power or optics transmission.

D. The high-voltage–electric-field system

The high voltage for the intense electric fields needed for the Stark absorption measurement was supplied by a precision 50-kV power supply (Spellman RHR-50P50). The danger of line broadening due to electric-field instability led to stringent limits on the time variation of the high voltage (see Sec. III B). This unit has specified drift 2×10^{-4}/h and ripple 2×10^{-4}. The voltage was measured via a high-impedance voltage divider, the readings from which agreed with the power supply front panel voltage setting to within 0.5%. This level is taken as the overall uncertainty in the applied voltage.

The electric field used for the Stark measurements was formed between two stainless-steel plates (50 mm long ×25 mm wide) bolted to insulating blocks. The spacing between the field plates (nominally 5 mm) was measured by inserting a series of precision-ground spacer rods between the plates.

Originally, the insulating structure was made from Teflon. However, it was found after several data-taking runs that, due to the softness of the Teflon, the plate spacing varied noticeably each time the structure was disassembled, cleaned, and reassembled (see below). After this was noticed, the range of variation of the plate spacing was determined by repeated disassembly and reassembly of the structure; this led to an assignment of the plate spacing for the runs taken with the Teflon insulating structure:

$$d(\text{Teflon structure}) = 5.39(13)\ \text{mm} \ . \tag{24}$$

To alleviate spacing variations, for the final data-taking run the insulating structure was rebuilt from Delrin, which is more mechanically stable than Teflon. This structure had the plate spacing

$$d(\text{Delrin structure})=4.98(3)\ \text{mm}\ . \tag{25}$$

As mentioned before, after ~8 h of operation, the deposition of thallium on the field plates became thick enough to cause both quasi-dc and transient discharges between the plates. Because of this, the electric-field structure was disassembled after each run; the plates were then cleaned with dilute nitric acid and the structure reassembled for the next run.

III. STARK-INDUCED AMPLITUDES OF THE $6P_{1/2}\to 7P_{1/2}$ TRANSITION

A. Overview of the experimental procedure

The absorption of 293-nm light due to the Stark-induced $6P_{1/2}\to 7P_{1/2}$ transition was measured as the laser was scanned through the ^{205}Tl $F=1\to F'=1$ resonance line. Each scan consisted of 20–30 points separated in frequency by ~40 MHz. At each point, the absorption was averaged over ~200 consecutive beam chop cycles (corresponding to a real time of ~3s). This led to a typical absolute uncertainty in μ_{293} of $\sim 5\times 10^{-5}$ per frequency point. The scan width covered the entire resonance line shape of a single isotope and hyperfine component of the transition and extended far enough into each wing of the line to determine the presence of any residual background. A typical scan through the Stark-induced resonance is shown in Fig. 4.

Two different procedures were used for the normalization of the 293-nm absorption signal by the 378-nm absorption signal. In both procedures, the 378-nm laser was scanned through resonance prior to each 293-nm scan. Each 378-nm scan consisted of 100 frequency points separated by ~10 MHz; at each frequency point, the absorption was averaged over 24 consecutive beam chop cycles. A typical 378-nm scan is shown in Fig. 5.

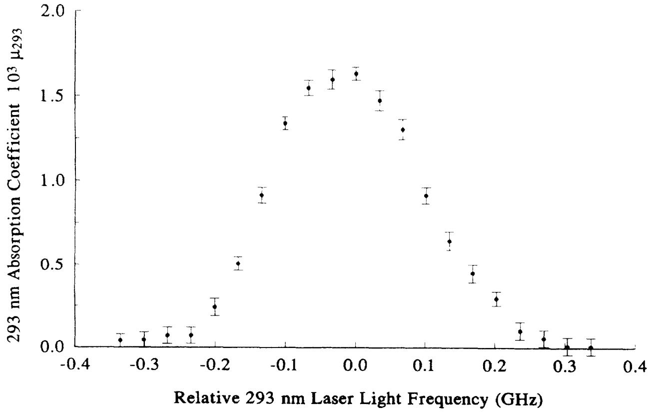

FIG. 4. A typical scan through the 293-nm Stark-induced ^{205}Tl $6P_{1/2}(F=1)\to 7P_{1/2}(F'=1)$ absorption resonance, with $E=80.1$ kV/cm, 293-nm laser light polarization $\boldsymbol{\epsilon}\|\mathbf{E}$, and Tl density corresponding to an absorption coefficient on the reference transition of $\mu_{378}(^{203}\text{Tl},\ F=1\to F'=0)\approx 3.5$. Each data point represents the average over 256 consecutive beam chops.

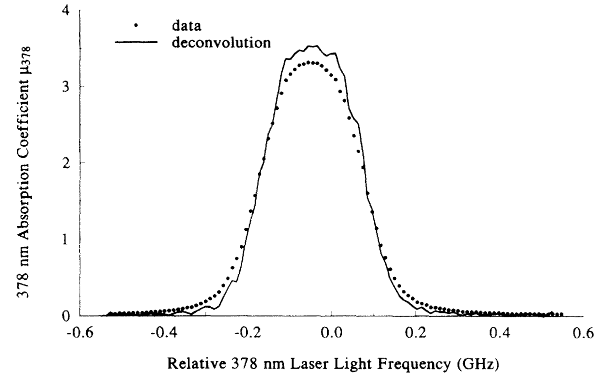

FIG. 5. A typical scan through the 378-nm ^{203}Tl $6P_{1/2}(F=1)\to 7S_{1/2}(F'=0)$ resonance used to normalize the Stark-induced absorption. The points show the experimental data; each point represents the average over 24 consecutive beam chops. The solid curve shows the result of the deconvolution of this data set from the Lorentzian line shape due to the natural width of the transition.

In one normalization procedure ("on-line normalization"), the 378-nm scans were used only to check the tuning of the 378-nm frequency. After each 378-nm scan, the line shape was fitted in order to find the frequency of the absorption peak and the 378-nm laser was tuned to this frequency. During the subsequent 293-nm scan, the ratio $\mu_{293}(\nu_{293})/\mu_{378}$ (peak) was computed for each beam chop. It was found that when the 378-nm laser was tuned to the peak of the absorption line, there appeared a small background in the observed 293-nm absorption. The cause of the background was not understood. However, because this background was never more than a few percent of the peak 293-nm absorption and could be determined accurately from the far off-resonant points in the 293-nm scan, it was not a serious limitation. (We make the reasonable assumption that this background was not affected by the tuning of the 293-nm light onto resonance.)

The other normalization procedure ("off-line normalization") was devised to eliminate the background in the 293-nm absorption which appeared when the 378-nm laser was on resonance. In this procedure, the 378-nm absorption used to normalize the data from a 293-nm scan was determined from the average of the peak absorptions of the 378-nm scans immediately preceding and following it. During the 293-nm scans, the 378-nm laser was tuned to a point ~500 MHz above line center. This procedure had the disadvantage that fluctuations in the atomic-beam density added to the noise in the relative absorption measurement.

With both normalization procedures, it was possible to determine the occurrence of a transient discharge in the high-voltage system directly from the 378-nm absorption data. Any change in the electric field led to a significant change in the 378-nm resonance frequency due to the dc

Stark shift. Such a frequency jump manifested itself as a large change in the observed 378-nm absorption either when the laser was tuned on resonance (in which case the absorption would diminish) or when the laser was tuned to the high-frequency wing of the line (in which case, since the dc Stark shift for this transition was negative, the absorption would increase). Any data point which showed evidence of a high-voltage instability was not considered in the subsequent analysis.

B. Line-shape considerations

The line shape of each transition (with a full width at half maximum of ~300 MHz for both transitions) was dominated by Doppler broadening due to the transverse velocity distribution of the atomic beam. If this were the only source of linewidth, the peak values of the line-shape functions $g(\nu-\nu_0)$ [see Eq. (11)] for the two transitions would be simply related by the ratio of the transition wavelengths

$$\frac{g_{378}(\text{peak})}{g_{293}(\text{peak})}=\frac{378}{293} \ . \tag{26}$$

There are, however, corrections to this relationship due to other contributions to the measured line shapes. The most important additional contribution to either of the measured line shapes was that due to the 21.1-MHz natural linewidth of the 378-nm transition. This contribution was removed by deconvolving the Lorentzian line shape due to spontaneous emission from the measured 378-nm absorption line shape. Data from a typical scan through one isotopic component (^{203}Tl) of the $F=1\rightarrow F'=0$ 378-nm resonance, along with the results from the deconvolution of this data, are shown in Fig. 5. The absolute frequency scale was determined by scanning over a wider frequency range and observing both isotopic components of the transition, the separation between which is known from the isotope and hyperfine structure of the $6P_{1/2}$ [13] and $7S_{1/2}$ [14] states. (See Sec. IV A for further details.) The "peak correction factor" C_{378}, defined as the ratio of the peak of the deconvolved line shape to that of the actual line shape, was determined from the deconvolution of a number of experimental 378-nm absorption profiles to be

$$\begin{aligned} C_{378} &\equiv \frac{g_{\text{deconvoluted}}(\text{peak})}{g_{\text{experimental}}(\text{peak})} \\ &= \frac{g_{\text{Doppler only}}(\text{peak})}{g_{\text{experimental}}(\text{peak})}=1.07(1) \ . \end{aligned} \tag{27}$$

The uncertainty in this value arises primarily from the fact that any noise in the experimental line shape is amplified in the deconvoluted line shape [15], but also includes the uncertainty from possible additional line broadening of the 378-nm transition due to the laser linewidth (nominally 1 MHz) and from possible errors in the absolute frequency scale calibration.

Broadening of the 293-nm transition due to the natural linewidth (2.6 MHz) [16,17] and to the laser linewidth (nominally 2 MHz) was considered and found to give corrections $\lesssim 0.5\%$. Defining C_{293} in a manner analogous to C_{378}, this implies

$$C_{293}=1.005(5) \ . \tag{28}$$

Thus we write the ratio of the peak values of the line-shape functions in Eq. (17) as

$$\frac{g_{378}(\text{peak})}{g_{293}(\text{peak})}=\frac{378}{293}\frac{C_{293}}{C_{378}} \ . \tag{29}$$

In the preceding discussion, it has been assumed that the Doppler effect is the only source of inhomogeneous broadening. In the conditions of this experiment, however, additional inhomogeneous broadening due to the nonuniformity (spatial or temporal) of the applied electric field was a serious concern because of the relatively large dc Stark shifts of the levels studied. At the largest electric fields used (~100kV/cm), Eq. (8) shows that deviations in E as small as $(\delta E/E)=3\times10^{-4}$ can in principle lead to additional broadening which is significant at the 1% level for the ~300-MHz-wide 293-nm transition. (In fact, the slight asymmetry of the 293-nm absorption line shape shown in Fig. 4 is believed to be due to spatial inhomogeneity of the electric field; see Sec. III D.) In order to guard against such systematic effects, measurements of the relative absorption were performed over a range of values of the applied electric field and the linearity of the relative absorption as a function of E^2 was checked.

C. Other systematic effects

A source of potential systematic errors was the spatial inhomogeneity of the atomic beam. Such inhomogeneity, in combination with imperfect spatial matching of the two laser beams, can cause systematic deviations in the relative absorption measurements. The homogeneity of the atomic beam was checked by comparing the peak 378-nm absorption at several different positions of the 378-nm laser beam. Using these data for the beam inhomogeneity and assigning a conservative limit for the range of spatial separation of the two laser beams, the systematic uncertainty in the relative absorption due to the effect was estimated to be $<1\%$. The overlap of the two laser beams was frequently checked during runs and occasionally adjusted to correct for small drifts.

Nonlinearity of the detection electronics for the 378-nm absorption was also a concern because of the large range of variation of the transmitted 378-nm signal, since the atomic beam had an optical thickness of several absorption lengths for this transition under normal running conditions. In order to minimize any possible effects due to this, the weakest isotope-hyperfine component of the 378-nm transition (the ^{203}Tl $F=1\rightarrow F'=0$ component) was used as the reference transition for all relative absorption measurements. In addition, the atomic-beam density was maintained such that μ_{378} (^{203}Tl $F=1\rightarrow F'=0)\leq 4$ (this was close to the maximum achievable optical thickness). In order to verify the linearity of the system over this dynamic range, the ratio of peak absorptions of two adjacent isotope components of the 378-nm transition was recorded over a wide range of beam densities up to $\mu_{378}=4$ for the largest component. The measured ratio was always found to be consistent with the value

$$\frac{\mu({}^{205}\mathrm{Tl})}{\mu({}^{203}\mathrm{Tl})}=\frac{70.5}{29.5}=2.39\ , \tag{30}$$

expected from the known natural abundance [18]. The measured value of this ratio, averaged over several data sets with widely varying beam densities, was 2.41(2) (the uncertainty was dominated by noise due to fluctuations in the beam density over the time of a scan). We use the standard value of Eq. (30) in our determination of α.

Possible systematic effects due to angular misalignments in the laser-beam linear polarization (see below) and laser-beam pointing (see Sec. II B), as well as due to residual elliptical polarization of the 293 laser (Sec. II B), were also considered [8]. These effects were found to give combined systematic uncertainties of $<0.5\%$ in the relative absorption measurement.

D. Results

Relative absorption data were taken in several different runs. In the course of each run, several data sets were taken at different values of the applied high voltage or the 293-nm linear polarization. Each data set consisted of approximately ten consecutive pairs of scans through the 378-nm resonance (^{203}Tl; $F=1\rightarrow F'=0$) and the 293-nm resonance (^{205}Tl; $F=1\rightarrow F'=1$).

In one of the runs, one data set was taken at each of ten values of the 293-nm polarization as the polarization was varied over a range of 90°. Off-line normalization was used in this run. The corresponding data are shown in Fig. 6. From Eq. (16), the expected dependence of the 293-nm absorption on the angle θ between the 293-nm polarization $\boldsymbol{\varepsilon}$ and the electric field $\mathbf{E}$ is given by

$$\mu_{293}(F=1\rightarrow F'=1)\propto 3\alpha^2\cos^2\theta+2\beta^2\sin^2\theta\ . \tag{31}$$

The data were therefore fitted to a function of the form

$$M(\theta_{\lambda/2})=A[\cos^2 2(\theta_{\lambda/2}-\varphi)+R\sin^2 2(\theta_{\lambda/2}-\varphi)]\ , \tag{32}$$

where $\theta_{\lambda/2}$ is the angle of the $\lambda/2$ plate relative to an arbitrary angular position on its rotary mount. The results of this fit determined the angle φ (i.e., the angle between the reference position on the $\lambda/2$ plate mount and position of this mount corresponding to $\boldsymbol{\varepsilon}\|\mathbf{E}$) to within 2°. In addition, from the fitted parameter $R=0.48(3)$ and Eq. (31), the ratio $|\beta/\alpha|$ is found to be

$$|\beta/\alpha|=\left[\frac{3R}{2}\right]^{1/2}=0.85(3)\ . \tag{33}$$

Once the angular alignment of the 293-nm polarization was determined, four separate runs were taken to determine the value of α to high precision. In runs 1–3, the off-line normalization method was used and the electric-field plates were held in the Teflon assembly. In run 4, the on-line normalization method was used and the electric-field plates were held in the Delrin assembly.

The value of α was determined from the relation of Eq. (17), modified to take into account the relationship of line-shape function peak values given in Eq. (29) and also to take into account the use of the less abundant isotope ^{203}Tl for the 378-nm absorption:

$$\alpha^2=\frac{C_{293}}{C_{378}}\,\frac{\mu_{293}|_{\mathrm{peak}}(F=1\rightarrow F'=1;\boldsymbol{\varepsilon}\|\mathbf{E};{}^{205}\mathrm{Tl})}{\mu_{378}|_{\mathrm{peak}}(F=1\rightarrow F'=0;{}^{203}\mathrm{Tl})}\,\frac{d^2}{V^2}\times\frac{a({}^{203}\mathrm{Tl})}{a({}^{205}\mathrm{Tl})}\,\frac{h}{192\pi^4}\lambda^3_{6P_{1/2}\rightarrow 7S_{1/2}}A(7S_{1/2}\rightarrow 6P_{1/2})\ . \tag{34}$$

Here d is the separation between the electric field plates, V is the applied voltage to the plates, and $a({}^{203}\mathrm{Tl})/a({}^{205}\mathrm{Tl})$ is the ratio of isotopic abundances.

In each run, a number of data sets were taken at various values of the applied electric field. The quantity Q defined by $Q\equiv[\mu_{293}(\mathrm{peak})/\mu_{378}(\mathrm{peak})]$ was plotted as a function of $E^2=(V/d)^2$ for each run to check for linearity. Two such plots are shown in Fig. 7, where the error bars are determined from the statistical deviation in $\mu_{293}(\mathrm{peak})/\mu_{378}(\mathrm{peak})$ (typically $\lesssim 1\%$ for the largest values of E) combined in quadrature with the uncertainty due to imperfect laser beam overlap (1%). As can be seen from Eq. (34), Q should be a linear function of E^2.

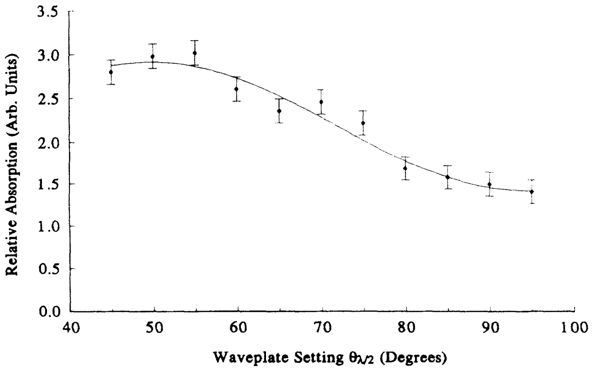

FIG. 6. Dependence of the Stark-induced absorption on the orientation of the $\lambda/2$ plate used to set the linear polarization of the 293-nm laser light. The curve is a fit to the expected dependence given by Eqs. (31) and (32).

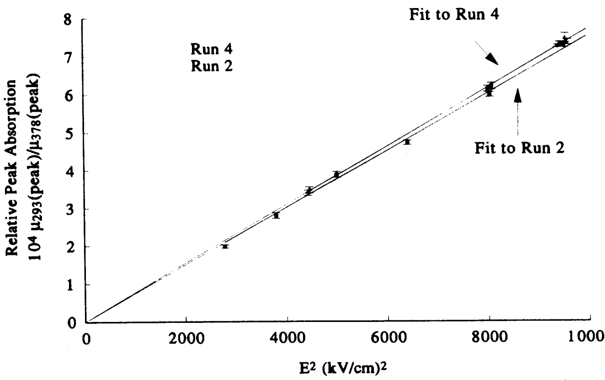

FIG. 7. Plot of ratio of peak absorptions $\mu_{293}(\mathrm{peak})/\mu_{378}(\mathrm{peak})$ vs the square of the applied electric field. Data from two runs are shown, as well as the least-squares fit to the data from each run.

Therefore, any systematic deviation from linearity of Q as a function of E^2 would indicate a systematic effect such as that due to an electric-field dependent component of the inhomogeneous broadening (see Sec. III B). Despite the noticeable (but relatively small) asymmetry in the 293-nm line shape at the highest values of the electric field (see Fig. 4), no such systematic variation was observed in the data from any of the runs at the level of $<0.5\%$. This implies that the observed line-shape asymmetry affected only the wings of the line and not the central region where the peak absorption is measured. This can be interpreted as evidence that the line-shape asymmetry was due to a small spatial inhomogeneity of the electric field near the edges of the atomic beam, where the transverse velocity is large and there is little contribution to the peak value of the line shape. This interpretation is consistent with expectations based on a calculation of the spatial variation of the electric field. (This calculation used an overrelaxation method solution to the Laplace equation [15].)

Because of the absence of systematic effects in the ratio of peak absorptions due to electric-field-induced inhomogeneous broadening, the values of the E-field-independent quantity $Q' \equiv Q/E^2$ from all data sets in each run could be averaged to form the quantity $\overline{Q}'_{\text{run}}$. The uncertainty in each value of $\overline{Q}'_{\text{run}}$ was assigned to be the quadrature sum of the statistical uncertainty determined from the variation of Q' within the run (typically $<0.5\%$) and the systematic uncertainty due to the electric-field plate spacing. For all runs, the uncertainty in $\overline{Q}'_{\text{run}}$ was dominated by the latter. The quantity $\overline{Q}'_{\text{total}}$ was determined from a weighted average of the four values of $\overline{Q}'_{\text{run}}$ (see Fig. 8):

$$\overline{Q}'_{\text{total}} \equiv \left\langle \frac{\mu_{293}(\text{peak})}{\mu_{378}(\text{peak})} \frac{d^2}{V^2} \right\rangle \bigg|_{\text{av}}$$

$$=7.58(14)\times 10^{-14}\ (\text{V/cm})^{-2}\ . \tag{35}$$

Finally, the value of $|\alpha|$ was extracted from Eqs. (27), (28), (30), (34), and (35), yielding

$$|\alpha| = 2.01(4)\times 10^{-5}\mu_B/(\text{V/cm})\ , \tag{36}$$

where the uncertainty is determined by adding in quadrature the uncertainties due to $\overline{Q}'_{\text{total}}$ (1.8%), C_{378} (1%), C_{293} (0.5%), the voltage calibration (0.5%), and $A(7S_{1/2}\rightarrow 6P_{1/2})$ (2.6%). The sign of α will be discussed below.

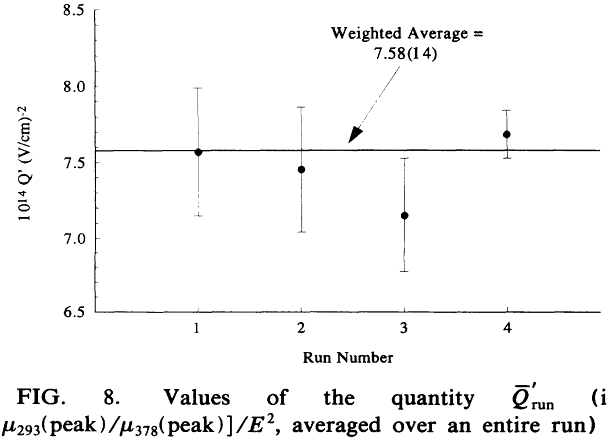

FIG. 8. Values of the quantity $\overline{Q}'_{\text{run}}$ (i.e., $[\mu_{293}(\text{peak})/\mu_{378}(\text{peak})]/E^2$, averaged over an entire run) for the four runs used to determine the value of α.

E. Discussion

The results obtained in this experiment differ significantly from those obtained in this laboratory using a similar technique. In Ref. [6], it was reported that $\alpha = 1.31(6)\times 10^{-5}\mu_B/(\text{V/cm})$. Because of this discrepancy, it seem worthwhile to speculate on possible systematic errors which may not have been considered in the analysis of that experiment. In order to do this, let us review briefly the methods of the previous measurement.

In Ref. [6], absorption due to the Stark-induced transition was measured using 293-nm laser light produced by frequency doubling of a cw-seeded pulsed laser amplifier system [19]. The ratio of transmitted intensity to incident intensity was measured at two frequency points: one on resonance and one 8 GHz off resonance. In addition, at each frequency point, this ratio was measured both with and without an applied electric field ($E\approx 1700$ V/cm). The measurements off resonance were considered necessary because of the presence of an electric-field dependent background. (This background was seen in the fluorescence accompanying the decay of the excited $7P_{1/2}$ state.) The linear dependence of the absorption on E^2 was verified.

The density of thallium in the vapor cell used as the absorption sample ($n\approx 10^{15}$ cm^{-3}) was determined by measuring the absorption of 535-nm light (produced with a cw dye laser) tuned to the $6P_{3/2}\rightarrow 7S_{1/2}$ $E1$ transition, in combination with a determination of the cell temperature (to determine the thermal population of $6P_{3/2}$ relative to $6P_{1/2}$) and cell length. For both transitions, the line shape was assumed to be due entirely to Doppler broadening. Using this line-shape model, α was extracted from the measured 293-nm absorption and the density, in combination with the known length of the electric-field plates.

We have considered many possible sources of systematic error not explicitly discussed in Ref. [6] and have rejected most of them as either inconsistent with the data reported there or insufficient to explain the discrepancy between the result reported there and our measurement. For instance, étalon effects in the optics which can in principle mimic a small absorption should be canceled by the comparison of E-on to E-off absorption both on and off resonance. Effects due to space-charge shielding of the applied electric field (which can arise from photoelectric emission from the field plates or from photoionization of Tl) should cause a deviation from the observed linear dependence of the 293-nm absorption on E^2. Absorption from the excited $7P_{1/2}$ state (inducing transitions to the continuum), which would lead to an E^2 dependence of the 293-nm absorption, is expected under the conditions of Ref. [6] to be small [8]; moreover, this would lead to an anomalously large apparent value of α rather than the anomalously small value reported.

One potentially serious systematic effect not considered in the analysis of Ref. [6] seems to us plausible as an explanation of the difference between the results reported there and our results. This effect is related to the full spectral profile of the pulsed 293-nm laser light used in Ref. [6]. There it was assumed that this light was contained in a bandwidth of ~200 MHz, which was considered negligible compared to the Doppler width of ~1.6 GHz. However, it has been noted on several occasions in recent work in this laboratory [20] that the visible output of the pulsed laser amplifier system (i.e., the output before doubling) has, in addition to the nominal spectral width, a large spectral pedestal with width ~30 GHz. In fact, the integrated intensity outside the narrow spectral peak of the pulse can account for $\sim\frac{1}{2}$ of the total intensity. Although the fraction of the intensity in this pedestal may be affected by the frequency-doubling process, it is plausible that the 293-nm light retains a similar spectral profile, since the laser intensities used were more than sufficient to saturate the doubling efficiency of the deuterated potassium dihydrogen phosphate (KD*P) crystal used. Obviously, if a large part of the spectral intensity of the light is outside the Doppler width of the transition, the observed absorption will be diminished; this would lead to an anomalously small apparent value of α.

The systematic effect just described should not, however, affect a measurement of the ratio $|\beta/\alpha|$ since the spectral width of the 293-nm light enters with the same multiplicative factor in the measurement of each Stark-induced amplitude separately. The ratio $|\beta/\alpha|$ was obtained in Ref. [6] both by the absorption technique and by measuring fluorescence resulting from excitation of the Stark-induced transition; in both cases, the appropriate signal was compared for the 293-nm light polarization $\boldsymbol{\varepsilon}\parallel\mathbf{E}$ and for $\boldsymbol{\varepsilon}\perp\mathbf{E}$. These techniques gave results consistent with each other [$|\beta/\alpha|=0.83(8)$ from absorption and $|\beta/\alpha|=0.83(1)$ from fluorescence], with the results reported here [Eq. (33)], and with an earlier result [3]. For these reasons, it is believed that the measurement of $|\beta/\alpha|$ reported in Ref. [6] (in particular, the more precise fluorescence measurement, which would not suffer from the systematic effect described above) is valid.

Let us now return to the results of the present work. The final result of Eq. (36) for $|\alpha|$ is in agreement with the theoretical prediction [4] for α [Eq. (4)], up to the sign ambiguity. We therefore assume that the theoretical sign is also correct and find

$$\alpha=2.01(4)\times10^{-5}\mu_B/(\mathrm{V/cm})\ . \tag{37a}$$

Using the result from Ref. [6] that the ratio $|\beta/\alpha|=0.83(1)$ (which is in agreement with both theory and the results obtained in this experiment, but more precise than either) and also the value of the sign of β/α from Ref. [3] (also in agreement with theory), the value of β is determined to be

$$\beta=1.67(4)\times10^{-5}\mu_B/(\mathrm{V/cm})\ . \tag{37b}$$

These results for α and β lead to a reinterpretation of the data from previous experiments which measured the ratios M/α [3] and $\mathrm{Im}(\mathcal{E}_P/\beta)$ [2], where M is the $M1$ amplitude and $\mathcal{E}_P$ is the parity nonconserving $E1$ amplitude of the $6P_{1/2}\rightarrow7P_{1/2}$ transition. The new measurements lead to the revised values

$$\begin{aligned}M&=-2.07(21)\times10^{-5}\mu_B\ ,\\ \mathrm{Im}(\mathcal{E}_P)&=-2.89(55)\times10^{-8}\mu_B\ .\end{aligned} \tag{38}$$

Both revised values are in reasonable agreement with theoretical predictions [4,21–23].

Finally, we would like to point out the general power of this technique for measuring weak transition amplitudes (including, e.g., the analogous Stark-induced amplitudes in Cs) to very high precision. The largest uncertainties arising from our experimental technique could clearly be reduced considerably with some effort. In particular, we note that (i) the statistical uncertainty could be reduced by using a higher-power laser beam for the weak transition, (ii) the uncertainty due to mismatch of the two laser-beam positions could be reduced by using array detectors to image each beam, (iii) the uncertainty due to line-shape corrections could be reduced by careful laser frequency calibration on the scale of the absorption line profile, and (iv) the uncertainty due to field plate spacing and voltage calibration could be reduced by careful construction. Because the largest single contribution to our final uncertainty arises from the uncertainty in the A coefficient for the reference $6P_{1/2}\rightarrow7S_{1/2}$ transition, we did not pursue these improvements. However, for many elements (in particular Cs) [24], the A coefficient for the principal resonance line is known to much better than 1%. Thus this source of uncertainty would be greatly reduced by using such reference transitions.

IV. dc STARK SHIFTS

A. The $6P_{1/2}\rightarrow7S_{1/2}$ transition

In order to measure the dc Stark shift of the $6P_{1/2}\rightarrow7S_{1/2}$ transition, the absorption of the 378-nm laser was recorded as the laser was scanned through both isotope components of the $F=1\rightarrow F'=1$ transition at different values of the applied electric field. (This hyperfine component was selected because it gives the maximum absorption and thus allows running at lower than usual Tl fluxes to minimize discharges in the high-voltage system.) The peak frequencies were determined by fitting the measured line shapes to Gaussians. Two typical scans and fits at different E fields are shown in Fig. 9. The absolute frequency scale was determined by comparison of the observed separation between isotopic components to the separation expected from previous precise determinations of isotope shifts and hyperfine constants for the $6P_{1/2}$ and $7S_{1/2}$ states [13,14]. The apparent isotope peak separation was observed to vary by $\lesssim1\%$ between scans at different values of E (i.e., with the peaks shifted significantly within the scan range); we take this as evidence that the absolute frequency calibration is determined to within 1%, including possible scan nonlinearities.

A graph of the position of the fitted peak frequencies vs E^2 is shown in Fig. 10. The graph shows the expected linear dependence. From the slope of this line, the dc

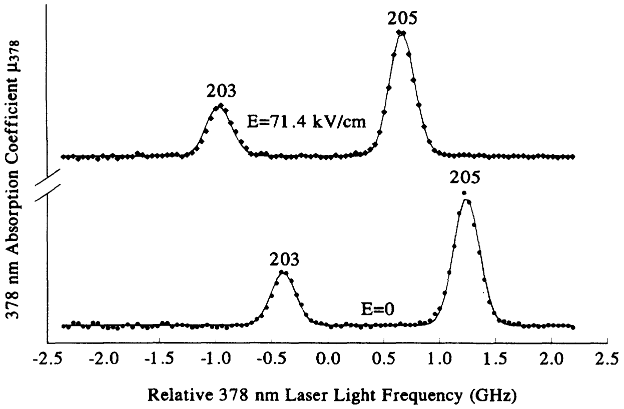

FIG. 9. Scans through the 378-nm $6P_{1/2}(F=1)\rightarrow 7S_{1/2}(F'=1)$ resonances used to determine the dc Stark shift. The two peaks in each scan corespond to the two isotopes ^{203}Tl and ^{205}Tl. Each data point represents the average over 24 consecutive beam chops. The solid lines represent a fit to the data, where for simplicity the line shape for each isotope is represented by a Gaussian.

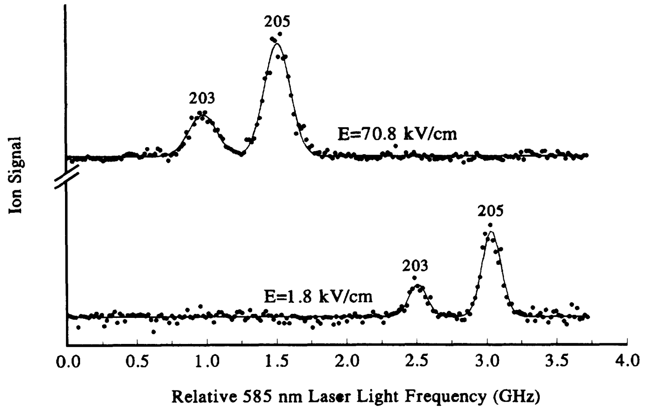

FIG. 11. Typical scans through the two-photon $6P_{1/2}\rightarrow 7P_{1/2}$ transition used to determine the dc Stark shift. Each data point represents the average over four consecutive laser pulses. The two peaks in each scan are the two isotopic components (^{203}Tl and ^{205}Tl) of the $F=1\rightarrow F'=1$ transition. The solid lines represent a fit to the data, where for simplicity the line shape for each isotope is represented by a Gaussian.

Stark shift is extracted:

$$\Delta\nu(6P_{1/2}\rightarrow 7S_{1/2})=-112(6)\ \mathrm{kHz}/(\mathrm{KV/cm})^2\ , \tag{39}$$

where the uncertainty is dominated by the uncertainty in the electric field calibration of 2.5% (the data were taken with the Teflon electric-field plate assembly). This result is in reasonable agreement both with a previous determination [25]

$$\Delta\nu(6P_{1/2}\rightarrow 7S_{1/2})=-96(10)\ \mathrm{kHz}/(\mathrm{KV/cm})^2 \tag{40}$$

and with the prediction from semiempirical theory [Eqs. (7) and (9)]

$$\Delta\nu_{\mathrm{theory}}(6P_{1/2}\rightarrow 7S_{1/2})=-104(30)\mathrm{kHz}/(\mathrm{kV/cm})^2\ . \tag{41}$$

B. The $6P_{1/2}\rightarrow 7P_{1/2}$ transition

The long integration times needed to achieve a reasonable signal-to-noise ratio in the absorption signal on the Stark-induced transition hampered the measurement of the $6P_{1/2}\rightarrow 7P_{1/2}$ transition Stark shift because of laser frequency instabilities. To avoid this difficulty, this shift was measured by observing the transition with a different technique, which gave an improved signal-to noise ratio.

For this measurement, a cw-seeded pulse-pumped laser amplifier [19] produced 585-nm light, which was used to excite the two-photon $6P_{1/2}\rightarrow 7P_{1/2}$ transition. The output pulses had $\tau\sim 5$ ns and contained a large intensity component with a bandwidth of ~ 150 MHz; a pulse energy of ~ 10 mJ was used. Absorption of a third photon from the same laser beam led to photoionization of the $7P_{1/2}$ state. The charge induced on the field plates in the electric-field assembly was converted to a voltage signal by a charge-sensitive preamplifier (Tennelec TC174).

The dc Stark shift was measured by scanning across the two isotopic components of the $F=1\rightarrow F'=1$ transition at various values of the electric field up to ~ 100 kV/cm. At each frequency point, the signal was aver-

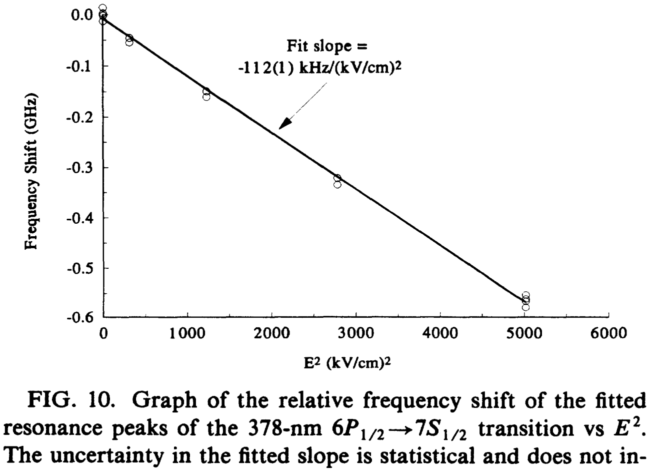

FIG. 10. Graph of the relative frequency shift of the fitted resonance peaks of the 378-nm $6P_{1/2}\rightarrow 7S_{1/2}$ transition vs E^2. The uncertainty in the fitted slope is statistical and does not include the 2.5% uncertainty in the electric field calibration (see text).

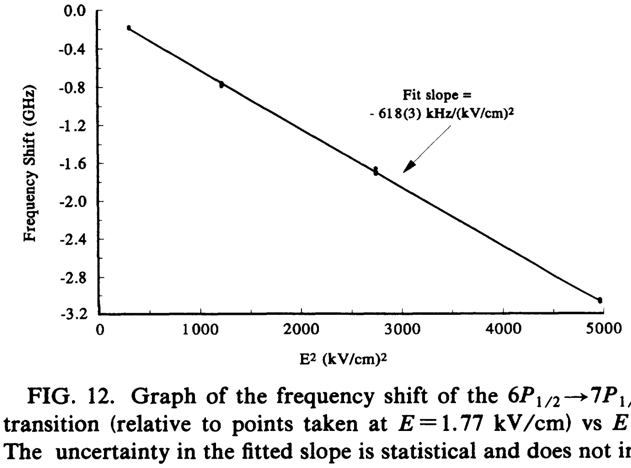

FIG. 12. Graph of the frequency shift of the $6P_{1/2}\rightarrow 7P_{1/2}$ transition (relative to points taken at $E=1.77$ kV/cm) vs E^2. The uncertainty in the fitted slope is statistical and does not include the 2.5% uncertainty in the electric-field calibration (see text).

aged over four laser pulses. Two typical scans at different values of electric field, along with the fitted curves used to determine the peak frequencies, are shown in Fig. 11.

The absolute frequency scale was determined to within 1% by comparison of the observed separation between isotopic components to the separation expected from previous precise determinations of hyperfine constants and isotope shifts for the $6P_{1/2}$ and $7P_{1/2}$ states [13,26]. A graph of the position of the fitted transition peaks vs E^2 is shown in Fig. 12. From the slope of the fitted line, the dc Stark shift is extracted:

$$\Delta\nu(6P_{1/2}\rightarrow 7P_{1/2}) = -618(31)\ \mathrm{kHZ/(kV/cm)^2}\ , \tag{42}$$

where the quoted uncertainty is again dominated by the uncertainty in the electric-field calibration. The prediction from semiempirical theory [Eqs. (7) and (8)] is

$$\Delta\nu(6P_{1/2}\rightarrow 7P_{1/2})_{\mathrm{theory}} = -614(13)\ \mathrm{kHz/(kV/cm)^2}\ , \tag{43}$$

in excellent agreement with the experimental result.

V. CONCLUSION

An intense atomic beam of thallium in the presence of a strong electric field has been used as an absorption sample to measure the Stark-induced amplitudes α and β for the $6P_{1/2}\rightarrow 7P_{1/2}$ transition in atomic thallium and also to determine the dc Stark shifts of the $6P_{1/2}\rightarrow 7P_{1/2}$ and $6P_{1/2}\rightarrow 7S_{1/2}$ transitions. These measurements serve as tests of complex calculations involving thallium wave functions. In all cases, the agreement between experiment and semiempirical theory is excellent. In the case of the Stark-induced amplitudes α and β, this measurement resolves a previous discrepancy between experiment and theory. In addition, the newly measured values of α and β lead to a reinterpretation of previous Stark-interference measurements of both the parity nonconserving amplitude and the $M1$ amplitude of the $6P_{1/2}\rightarrow 7P_{1/2}$ transition.

ACKNOWLEDGMENTS

The authors are grateful to Max Zolotorev for many useful discussions and also for his contributions to the development of the atomic beam source. This work was supported by National Science Foundation Grant No. PHY-9111771.

---

[1] C. E. Moore, *Atomic Energy Levels,* Natl. Bur. Stand. (U.S.) Cir. No. 467 (U.S. GPO, Washington, DC, 1958), Vol. III.
[2] P. S. Drell and E. D. Commins, Phys. Rev. A **32**, 2196 (1985).
[3] S. Chu, E. D. Commins, and R. Conti, Phys. Lett. **60A**, 96 (1977).
[4] D. Neuffer and E. D. Commins, Phys. Rev. A **16**, 844 (1977).
[5] W. R. Johnson *et al.*, Phys. Rev. A **32**, 2093 (1985).
[6] C. E. Tanner and E. D. Commins, Phys. Rev. Lett. **56**, 332 (1986); C. E. Tanner, Ph.D. thesis, University of California at Berkeley, 1985.
[7] V. V. Flambaum and O. P. Sushkov, J. Quant. Spectrosc. Radiat. Trans. **20**, 569 (1978).
[8] D. DeMille, Ph.D. thesis, University of California at Berkeley, 1994.
[9] A. Yariv, *Quantum Electronics* (Wiley, New York, 1989).
[10] J. C. Hsieh and J. C. Baird, Phys. Rev. A **6**, 141 (1972).
[11] A. Gallagher and A. Lurio, Phys. Rev. **136**, 87A (1964).
[12] J. B. Anderson, in *Molecular Beams and Low Density Gasdynamics,* edited by P. P. Wegener (Dekker, New York, 1974).
[13] A. Berman, P. Kusch, and A. K. Mann, Phys. Rev. **77**, 140 (1950); A. Berman, *ibid.* **86**, 1005 (1952).
[14] G. Hermann, G. Lasnitschka, and D. Spendgler, Z. Phys. D **28**, 127 (1993).
[15] W. H. Press *et al.*, *Numerical Recipes* (Cambridge University Press, New York, 1986).
[16] L. Hunter, E. Commins, and L. Roesch, Phys. Rev. A **25**, 885 (1982).
[17] J. V. James, C. C. Wang, and C. Guo, Phys. Rev. A **32**, 643 (1985).
[18] *CRC Handbook of Chemistry and Physis,* edited by R. C. Weast (CRC Press, Boca Raton, FL, 1981).
[19] P. S. Drell and S. Chu, Opt. Commun. **28**, 343 (1979).
[20] D. Budker, D. DeMille, E. D. Commins, and M. Zolotorev (unpublished).
[21] V. A. Dzuba *et al.*, J. Phys. B **20**, 3297 (1987).
[22] A. C. Hartley, E. Lindroth, and A.-M. Martensson-Pendrill, J. Phys. B **23**, 3417 (1990).
[23] A. C. Hartley and P. G. H. Sandars, J. Phys. B **23**, 4197 (1990).
[24] C. E. Tanner *et al.*, Phys. Rev. Lett. **69**, 2765 (1992).
[25] T. R. Fowler and J. Yellin, Phys. Rev. A **1**, 1006 (1970).
[26] M. Grexa *et al.*, Phys. Rev. A **38**, 1263 (1988).

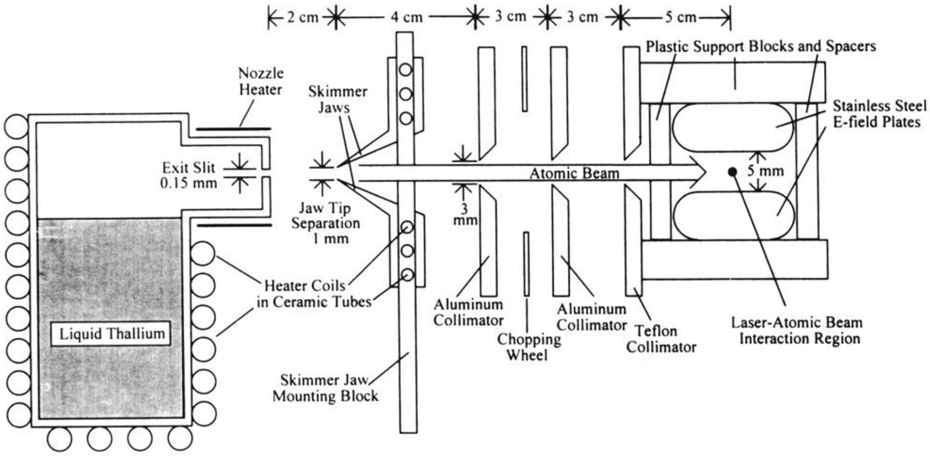

FIG. 2. Schematic depiction of the atomic beam oven, collimators, and interaction region. All distances shown are approximate.